Bulletin of the Mineral Research and Exploration

http://bulletin.mta.gov.tr

Geological and reservoir modelling of coalbed methane in Karadon Region of Zonguldak Basin (Türkiye): A case study

Muhammed Emin BULGUROĞLU[*a] , Ali SARI[b] , Sofiane BELHOCINE[a] , Mehmet Sıddık KIZIL[c] , Turhan AYYILDIZ[b] and Demet Banu KORALAY[d]

[a] *Turkish Petroleum Corporation, Production Department, 06510 Çankaya, Ankara, Türkiye*

[b] *Ankara University, Faculty of Engineering, Department of Geological Engineering, 06830 Gölbaşı, Ankara, Türkiye*

[c] *The University of Queensland, Faculty of Engineering, School of Mechanical and Mining Engineering, 4072, St Lucia, Queensland*

[d] *Pamukkale University, Faculty of Engineering, Department of Geological Engineering, 20160, Denizli, Türkiye*

Research Article

ABSTRACT

The Zonguldak Basin stands out as Türkiye's primary hub for bituminous coal production alongside a notable coalbed methane content of mined coal seams. In this study, we are proposing for the first time an integrated approach of geological modelling, reservoir characterization, and production forecasting of one coalbed methane block within Zonguldak Basin to understand the potential of this unconventional resource. The study initiated with the development of a 3D geological model data from the Karadon coal mine. Results of several laboratory tests conducted on coal samples such as desorption capacity which is measured as 666.67 scf/ton is integrated into the model. A reservoir model was developed by incorporating gas composition, pressure-volume-temperature (PVT) characteristics, and special core analysis (SCAL) data. A combination of 1,2,3,4 and 5 wells scenarios is proposed to figure out the best production solution adapted to the study area. As a result, a 5-wells configuration also known as the "5 spot wells" layout is selected. Five wells will be in the same well pad but deviated 600 meters distance in target zones. Each well in the pad includes two frac stages at two separated coal and shale interbedded intervals. The final volumetric projection suggests a cumulative gas production estimates around 1.803 billion m³ from 5 wells, which confirms the potential of coalbed methane as an important additional energy resource to Türkiye's economy.

1. Introduction

The methane potential inherent in the coal reserves of the Zonguldak Basin has been well-documented over the years by various researchers (Yalçın et al., 1994, 2002; Serpen et al., 1998; Gürdal and Yalçın, 2000; Hoşgörmez, 2007; Sıyanuç and Gümrah, 2009; Barış et al., 2016; Baltaş, 2018). Dating back to 1848, coal extraction has been a longstanding practice

in the Zonguldak Basin. However, the region has experienced a number of mine accidents as evidenced by the occurrence of 90 unexpected gas and coal explosions between 1969 and 2013, primarily in the Kozlu and Karadon Collieries. These tragic incidents resulted in 374 fatalities and 113 injuries (Fişne and Esen, 2014). More recently, 14th of October 2022, there has been another gas explosion in coal mine

Corresponding author: Muhammed Emin BULGUROĞLU, muhammedeminbulguroglu@gmail.com

located in Bartın-Amasra with 41 fatalities. In light of these events, numerous researchers have to assess the coal bed methane potential within the Zonguldak Basin. Their aim was twofold: to mitigate the risk of accidents inherent in deepening coal mining operations, and to elevate methane gas production to an economically viable level by unlocking the untapped economic potential of methane extraction from coal beds in the region.

This article marks an initial effort in conducting the first-ever Coal Bed Methane (CBM) reservoir characterization and simulation project within the Karadon area. While numerous similar coal reserve assessments have been undertaken in recent years, they primarily focused on specific regions within the broader Zonguldak Basin. For instance, previous studies by Serpen et al. (1998) and Sıyanuç and Gümrah (2009) investigated the CBM potential within the Zonguldak Basin and the Amasra Coal Region, respectively. Serpen et al. (1998) adopted a stochastic approach, employing Monte Carlo simulation to preliminarily evaluate gas production potential in the Zonguldak Basin. Their findings indicated a wide range of in-situ coalbed methane reserves, spanning from 1.5 billion to 7 billion m³, with an expected value of 4.8 billion m³ (P50). On the other hand, Sıyanuç and Gümrah (2009) employed a statistical CBM reserve estimation method for individual coal seams in the Amasra region, utilizing Monte Carlo simulations. Their analysis yielded estimates of possible reserves (P10) of 2.07 billion m³, probable reserves (P50) of 1.35 billion m³, and proven reserves (P90) of 0.86 billion m³. Furthermore, Barış et al. (2016) undertook a CBM gas potential estimation specifically within the Amasra region, located in the eastern part of the Zonguldak Basin. Their study drew data from a private company actively involved in CBM exploration projects in the region. Planning encompassed the deployment of 49 vertical wells within a drainage area of 0.16 km² (40 acres) across two designated license areas. Additionally, 23 multi-lateral well profiles were established for comparative analysis within the same area. Employing the Generalized Equation-of-State (GEM) program from the Computer Modelling Group (CMG), they forecasted 20 years of gas production. The cumulative gas production estimates

for the vertical wells totalled 0.617 billion m³, with an additional 0.523 billion m³ attributed to the multi-lateral wells within the two license areas.

The vast expanse of the Zonguldak Basin, spanning 3,885 km², poses a challenge for comprehensive CBM studies. To yield meaningful insights, such investigations necessitate concentration in areas abundant with data and conducive to understanding coal continuity. Barış et al. (2016) exemplified this approach in their pioneering work within the Amasra region, production forecasts were derived from data gathered from 49 vertical wells within a roughly 10 km² area. While these localized studies may yield smaller gas in place values compared to basin-wide calculations, they offer more realistic outcomes. Following a similar rationale, this study focuses on the Karadon region, situated further west of Amasra within the Zonguldak Basin. Unlike Amasra, Karadon boasts an operational coal mine managed by the Turkish Hard Coal Enterprise, providing ample underground data. Moreover, this study incorporates geological modeling and reservoir simulation. The geological complexity of the region, characterized by active tectonism resulting in steeply dipping coal seams, poses significant challenges. Additionally, the paralic nature of the Zonguldak Basin—dominated by river systems—further complicates coal seam continuity assessment. Consequently, attempting to calculate CBM potential basin-wide proves formidable. In light of these challenges, this study focuses on a pilot area within the Karadon region, leveraging available underground data. The geological model, enriched by laboratory analysis of coal samples from Karadon, serves as a reasonable foundation. Field visits facilitated the identification of optimal well locations and configurations, enriching the dataset employed in this study. The methodology followed in this study can also be applied to other blocks in the Karadon region. Thus, static, and dynamic reserve calculations can be made realistically in high resolution, from small to large scale.

2. Material and Method

The study area, as shown in Figure 1, lies within the western region of the Black Sea in Türkiye, situated to the northeast of Zonguldak's city centre.
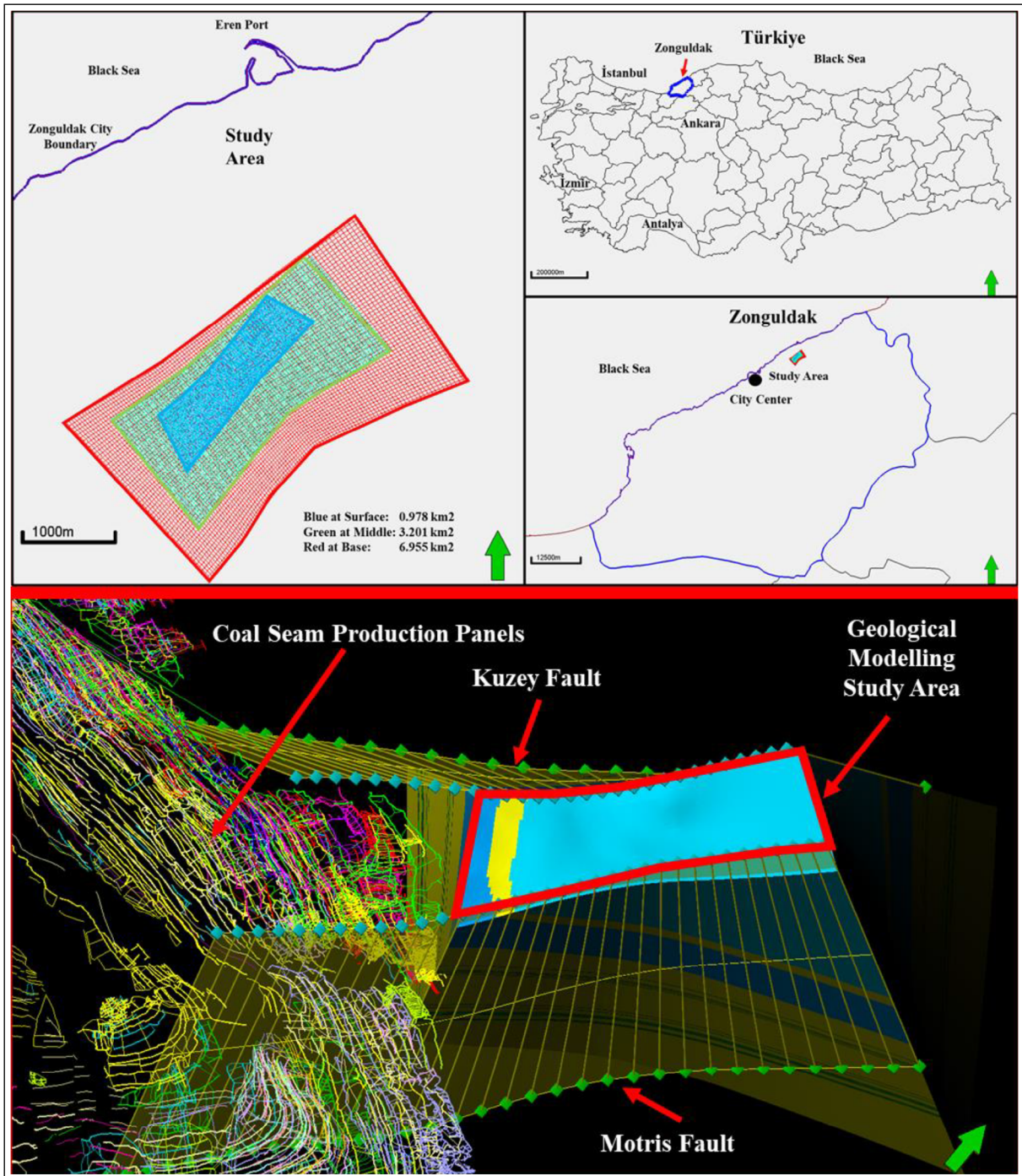
Figure 1- Location of study area in Türkiye-Zonguldak and The view of geological modelling study area from above with the coal galleries, Motris and Kuzey faults.

Notably, the area exhibits a gradual reduction in size from its deeper segments to the surface.

Figure 2 illustrates the Generalized Stratigraphy portraying the geological layers within the studied block, highlighting the coal seams and shales associated with coal seams pivotal to this research. Different blocks have different number of coal seams. To make it more local, only coal seams and formations present in the studied block has been shown in the Figure 2. Foundational to the Zonguldak Basin are Carboniferous-aged units, with the Namurian aged

Era	System	Stage	Stratum	Formation	Lithology	Coal Seams	Explanation
Mesozoic	Cretaceous	Lower Cretaceous	Aptian	Kapuz		No Coal	Limestone
			Lower Aptian	İncüvez			Interbedded conglomerate, sandstone, claystone
			Barremian	Zonguldak			Limestone, dolomitic limestone, sandstone
Paleozoic	Carboniferous	Upper Carboniferous	Westphalian BC	Karadon		Very Thin Coals	Interbedded sandstone, siltstone, coal seams and conglomerate
			Westphalian A	Kozlu		Büyük	Coal Seam with Interbedded claystone, sandstone and conglomerate
						Akdağ	Coal Seam with Interbedded claystone, sandstone and conglomerate
						Unudulmuş	Coal Seam with Interbedded claystone, sandstone and conglomerate
						Domuzcu	Coal Seam with Interbedded claystone, sandstone and conglomerate
						Kurul	Coal Seam with Interbedded claystone, sandstone and conglomerate
						Hacımemiş	Coal Seam with Interbedded claystone, sandstone and conglomerate
						Sulu	Coal Seam with Interbedded claystone, sandstone and conglomerate
						Acılık	Coal Seam with Interbedded claystone, sandstone and conglomerate
						Çay	Coal Seam with Interbedded claystone, sandstone and conglomerate
			Namurian	Alacaağzı		Very Thin Coals	Claystone, siltstone, sandstone
			Visean	Yılanlı		No Coal	Limestone **Unscaled**

Figure 2- Generalized Stratigraphy of the block located in Karadon region showing geological layers present in study area, and the coal seams used modelled for this research.

Alacaağzı Formation overlaying the Visean aged Yılanlı Formation at its base. Above, the Westphalian A aged Kozlu Formation, housing the primary coal-bearing formations, rests atop the Namurian-aged strata, succeeded by the Westphalian B-C-D aged Karadon Formation. Here, Carboniferous-aged coal-bearing formations are superimposed by Cretaceous-aged deposits, notably the Zonguldak Formation limestones. This juxtaposition is marked by an unconformity, highlighting a significant geological transition. Subsequently, the Lower Aptian-aged İncüvez sandstone and the Aptian-aged Kapuz Formation limestones crown the geological sequence, adding further complexity to the stratigraphic framework of the region.

2.1. Geological Modelling

Geological modelling in the study was conducted utilizing Schlumberger's Petrel software (version 2022.1), a widely employed tool in the oil industry. This software is renowned for its seamless integration with Schlumberger's Eclipse platform, facilitating efficient transfer of geological models for reservoir simulations. In the designated study area of the Karadon region, a coal mine operated by the Turkish Hard Coal Enterprises—a state institution—provides valuable data such as underground mine coal production data and measured fault angles. By accessing the coordinates of coal production panels spanning the entire area, a comprehensive understanding of the geological landscape was attained. Nine consistent coal seams have been identified between the Motris and Kuzey 1 faults (Figure 2), the focal area for our modelling endeavours. The assessment of fault characteristics, including the dipping angle and direction, was facilitated by data gathered from coal galleries. Notably, coal production ceased near fault lines, aiding in the determination of fault offsets. The Kuzey 1 Fault displays a northwest dip angle ranging from 70 to 80 degrees, while the Motris Fault exhibits a southeast dip angle within the same range. These faults collectively create a graben, lifting the block approximately 150-200 meters. While underground data was unavailable for the study area,

surface geology maps were utilized to extrapolate fault patterns and angles. This approach allowed for informed interpretations of fault behaviour within the geological model.

Precise thickness measurements of coal and shale were extracted from the operational plans prepared by the Turkish Hard Coal Enterprises. In this geological modelling endeavour, which entails breaking down units into manageable segments for subsequent reservoir simulation, particular emphasis was placed on coal and shale lithologies, recognized as primary sources of methane gas. Notably, where coal-bearing formations exhibit regular stacking, organic-rich shale lithologies are consistently found above and below the coal seams. However, occasional transitions directly to sandstone were observed, indicating geological complexities. Moreover, it was noted that certain coal seams encompass more than one coal-shale zone, illustrating the intricate layering within the formations. To organize this data comprehensively, each coal, shale and sandstone is gathered as a table, incorporating insights gleaned from coal production records. Facies modelling incorporated coal and shale units from the Westphalian A-aged Kozlu Formation, featuring coal thicknesses ranging between 2 and 5 m and shale thicknesses varying between 2 and 10 m, totalling 70 and 74 m, respectively (Figure 3).

Upon scrutinizing digital data of coal seam production along the production floors, a noticeable sloping pattern emerges as seen in Figure 4. These slopes were meticulously analysed for each coal seam individually, revealing a consistent north-eastward dip across all seams within this block. On average, these coal seams exhibit a 45-degree slope. In alignment with the coal seams, both the shale layers below and above them were also modelled with a 45-degree dip in the same north-eastward direction.

The delineation of the geological model's boundaries was accurately executed, with the interpreted Motris and Kuzey faults demarcating the north-south boundary, while the western boundary was determined by the furthest extent of coal production galleries. Conversely, the eastern boundary of the model was established at a distance of 2,000 m from the designated western limit (Figure 4). Beyond this delineation, geological units plunge to depths where model realism becomes dubious. For the grid division process, increments of 25 m were adopted for both the I and J axes for geological modelling. When segmenting geological units into layers, coal formations were subdivided into sections as thin as 1 m, to capture intricate details. Meanwhile, shale units were partitioned into sections of at least 2 m, ensuring a balance between detail and computational efficiency.

2.2. Reservoir Modelling

In contrast to conventional reservoirs, the unconventional coal reservoir is typically simulated using a double porosity system, comprising both pores and fractures. The macroporosity system encompasses the natural fractures within the coal known as cleats, while the microporosity system pertains to the minuscule pores within the coal matrix.

Cleats manifest in two primary forms: Face cleats and butt cleats. Face cleats are typically the initial fractures to form in coal rocks, exhibiting continuity, while butt cleats develop subsequently between two parallel face cleats (Laubach et al., 1998). These two cleat systems intersect perpendicularly, defining the permeability pathways crucial for gas flow within the coal formation (Puri et al., 1991). Though the coal matrix itself possesses minimal permeability, hindering gas flow, the cleat system serves as the primary conduit for desorbed gases to migrate towards production wells. Understanding the intricacies of the cleat system is paramount for optimizing coalbed methane production, as it determines the potential yield of gas from the reservoir (Laubach et al., 1998).

The software tools employed for estimating coalbed methane production forecasts encompass Petrel Reservoir Engineering and Eclipse. Petrel Reservoir Engineering primarily facilitated the dynamic model's preparation (pre-processing) and subsequent data plotting and analysis (post-processing). Eclipse, on the other hand, served as the main engine—a 3D reservoir simulator tasked with simulating gas flow within the coal system, estimating phase saturations, pressures, and ultimately, forecasting production. However, a notable limitation of this model lies in its inability to accommodate changes in porosity

Era	System	Stage	Stratum	Formation	Coal Seam Zone	Lithology	Thickness (meters)
Mesozoic	Cretaceous	Lower Cretaceous	Aptian	Kapuz	No Coal	Limestone	Changes through model
			Lower Aptian	İncüvez		Sandstone	100
			Barremian	Zonguldak		Limestone	400
Paleozoic	Carboniferous	Upper Carboniferous	Westphalian BC	Karadon	Very Thin Coals	Sandstone	250
			Westphalian A	Kozlu	Büyük	Shale	3
						Coal	5
						Shale	2
					Sandstone	Sandstone	60
					Akdağ	Shale	3
						Coal	5
						Shale	2
						Coal	4
					Sandstone	Sandstone	11
					Unudulmuş	Shale	3
						Coal	5
						Shale	2
					Sandstone	Sandstone	15
					Domuzcu	Shale	3
						Coal	5
						Shale	2
					Sandstone	Sandstone	410
					Kurul	Shale	2
						Coal	5
						Shale	3
					Sandstone	Sandstone	30
					Hacımemiş	Shale	2
						Coal	5
						Shale	3
					Sandstone	Sandstone	50
					Sulu	Shale	5
						Coal	5
						Shale	3
						Coal	3
						Shale	2
						Coal	2
					Acılık	Shale	10
						Coal	5
						Shale	5
						Coal	3
						Shale	3
						Coal	2
						Shale	2
					Sandstone	Sandstone	50
					Çay	Shale	2
						Coal	5
						Shale	3
						Coal	4
						Shale	4
						Coal	4
						Shale	2
						Coal	3
						Shale	3
					Sandstone	Sandstone	480

Figure 3- Kozlu, Karadon, Zonguldak, İncüvez and Kapuz Formations facies distrubiton of individual layering and thicknesses of zones.
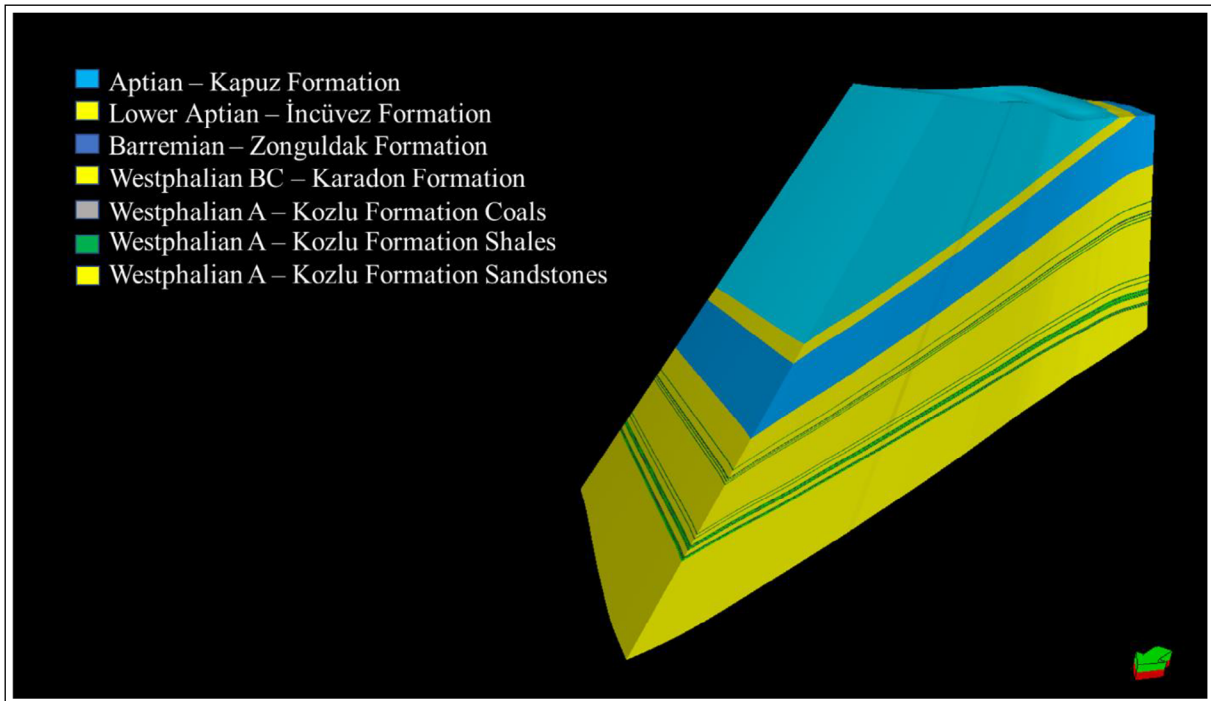
Figure 4- All modelled geological units and their angles. Unscaled due to 3D view of Petrel.

and permeability resulting from matrix shrinkage and swelling during coal sorption (Warren and Root, 1963). The Eclipse model is structured into two distinct systems: the matrix system, representing the coal, and the permeable fracture system, illustrating the cleat network.

Understanding the gas composition and Pressure-Volume-Temperature (PVT) characteristics of CBM is pivotal, as it profoundly impacts every stage of the project, spanning from exploration to enhanced gas recovery via gas injection. While methane (CH_4) predominates in coal gases, other constituents such as ethane (C_2H_6), propane (C_3H_8), carbon dioxide (CO_2), nitrogen (N_2), and water (H_2O) may also be present, released during the coalification process. The cumulative methane formation during coalification ($R0$ max 0.5-1.8%) typically ranges between 56.6 and 141. m^3/t (Scott et al., 1994).

In the Karadon region, numerous PVT samples have been collected from early drilled exploration wells, followed by chromatography analysis to discern the gas composition and PVT characteristics. The findings from these laboratory experiments clearly establish methane as the predominant component of Zonguldak coalbed gas, constituting over 95% of the composition. While other hydrocarbon and non-hydrocarbon components are present, their concentrations remain notably low.

Based on the chromatography, BlackOi PVT correlations have been developed and tested to generate the PVT model for Karadon coal sample. The correlations would help to define the gas behaviour with pressure changes under reservoir conditions. At initial reservoir pressure by default (Figure 5): Initial Gas Formation Volume Factor (FVF): 0.0067 rm^3/m^3, Initial gas viscosity: 0.16 Cp.

The Darcy's Law governs the flow of free gas into the pore system, similar to conventional reservoirs. However, in most CBM projects, the contribution of free gas production to the total CBM production remains minimal, typically not exceeding 2% even under optimal conditions. The primary source of gas production in coalbed methane projects arises from gas adsorbed on the coal surfaces. Coal exhibits an adsorption capacity, quantified as the volume of adsorbed gas in standard cubic feet divided by the mass of coal in tons. The magnitude of gas adsorption primarily hinges on coal quality. This relationship between gas pressure and coal capacity, or methane
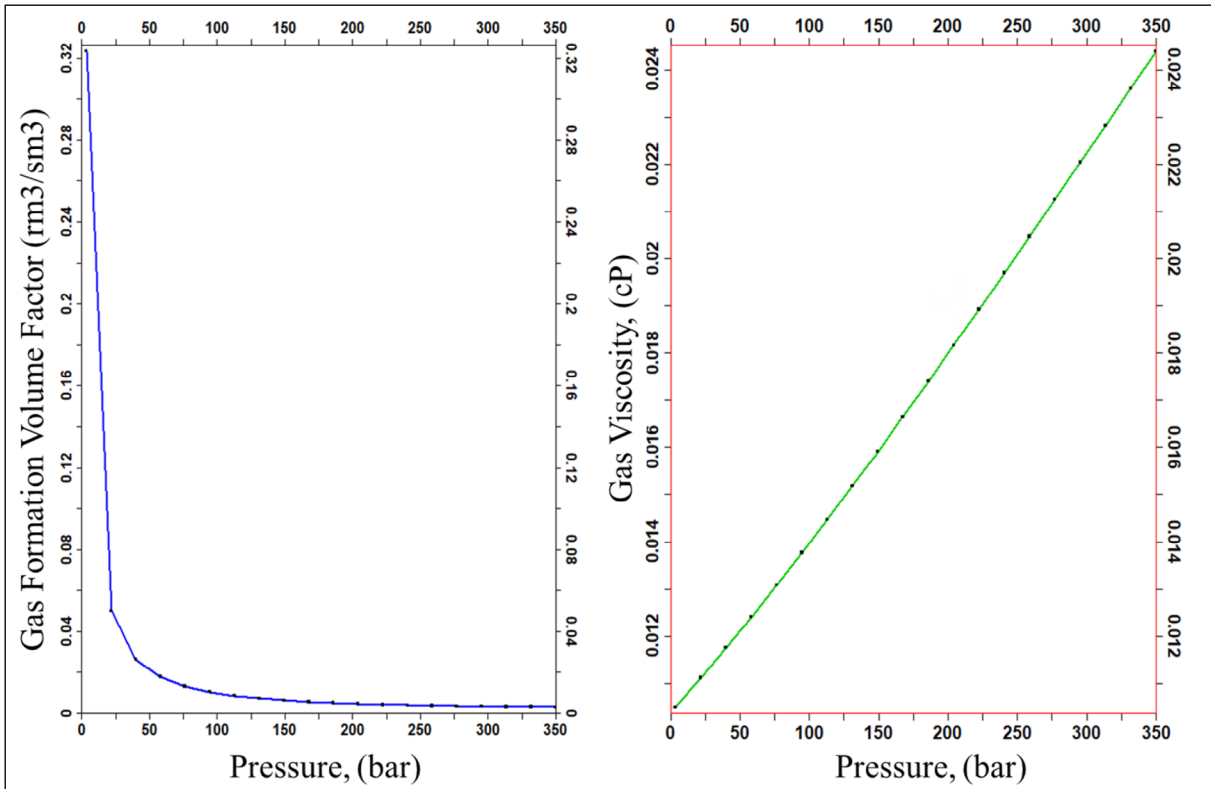
Figure 5- Calculated formation volume factor and viscosity for reservoir simulation study.

volume at constant temperature, is elucidated through Sorption or Adsorption Isotherms.

Numerous laboratory experiments concerning total gas content and gas desorption have been conducted in the Karadon area. One representative adsorption result is selected and it reveal a methane storage capacity of 666.67 scf/ton as received (equivalent to 18.87 m³/ton) (Figure 6). The pressure differential resulting from gas adsorption was measured, and employing the Langmuir Isotherm adsorption model, the quantity of gas adsorbed as a function of pressure was determined.

The previously mentioned methane storage capacity has been adjusted to account for mineral and moisture fractions, which have been measured for various coal samples at 10% and 3%, respectively. The average density of coal, derived from both log and core data, is recorded as 1,430 kg/m³.

The Langmuir equation 1 (Langmuir, 1918), is represented as follows:

$$Q=(VL*P)/(PL+P) \qquad (1)$$

In addition to coal, extensive research has been conducted in Zonguldak regarding the shale layers, with indications suggesting the potential for methane saturation within these formations, thus offering an additional contribution to total gas production (Yalçın and İnan, 2002). However, due to the absence of direct measurements on the shale samples, default values from Petrel were utilized, assuming lean shale gas concentration. Figure 6 depicts the Langmuir isotherm applied to the shale layers, where the total gas capacity is estimated to be four times lower than that of the coal system. While shales are increasing the total production of gas values, it is not significant amount comparing to coals.

Special core analysis (SCAL) data or relative permeability curves are paramount parameters that dictate the deliverability of gas and water from the coal system. Clarkson et al. (2011) underscored the significance of relative permeability curves in gauging coal seam gas production performance. Relative permeability delineates the multiphase flow within porous media, elucidating the alterations in each phase
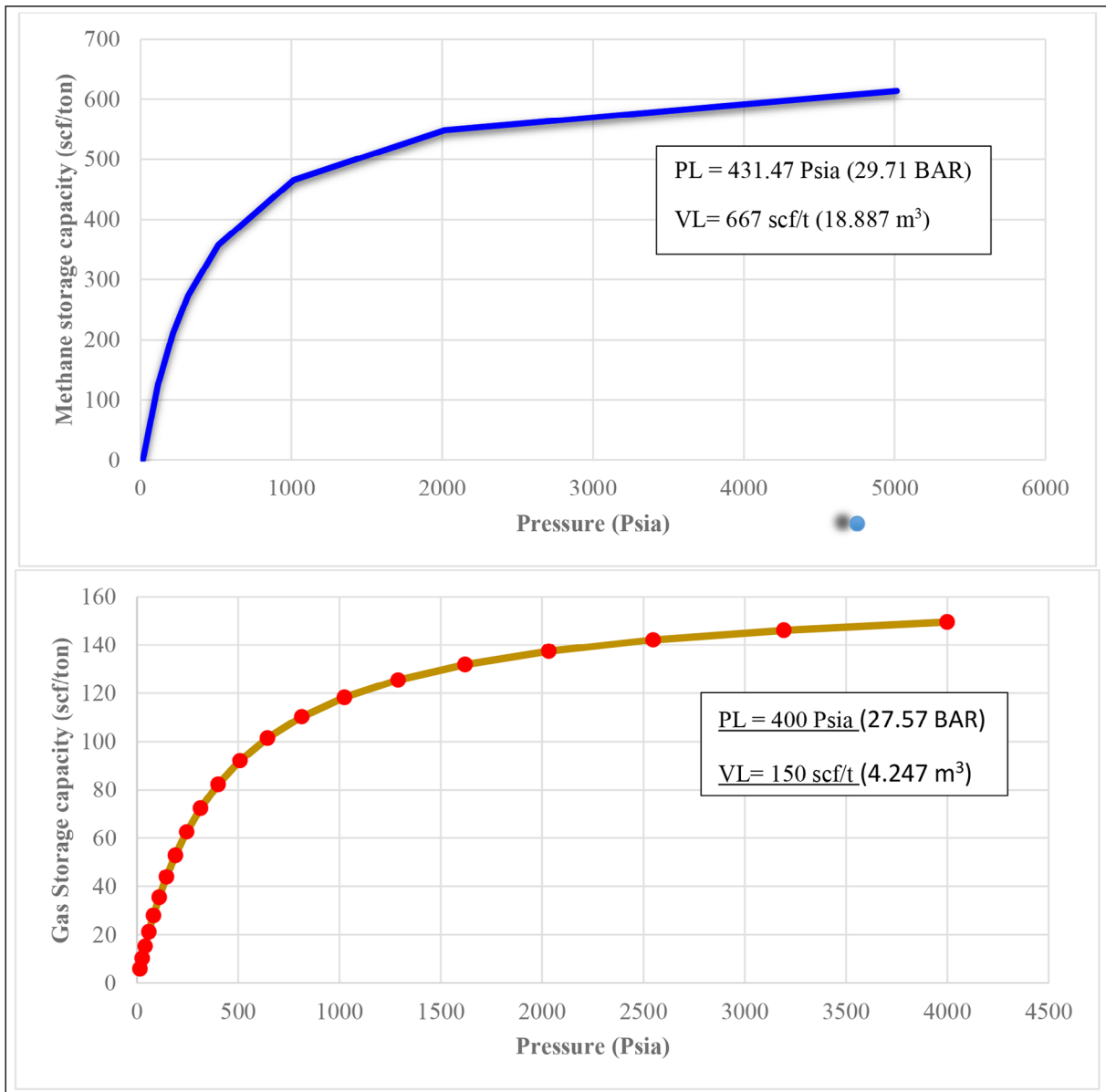
Figure 6- The results of Langmuir coal isotherm and the default results of shale adsorption data.

saturation. Evidence from early drilled wells in the Karadon field suggests that the cleat system initially exhibits 100% water saturation. To define the relative permeability curves for the coal and shale systems, Corey relative permeability functions were employed. These functions provide valuable insights into the dynamic behavior of gas and water flow within the coal and shale formations.

Figure 7 shows the two relative permeability functions used respectively for the coal and shale systems. Coal Relative permeability is modified from Law et al. (2002) and shale relative permeability is

taken from Petrel shale default values. For the cleat system, and per other references from worldwide case studies, straight lines relative permeability curves have been used. It represents natural fractured system. Table 1 shows details of the relative permeability data used in this study.

In the pursuit of evaluating various field development scenarios for the Karadon study area reservoir model, a dynamic model has been constructed. This model incorporates geological heterogeneities, integrating data from adsorption, PVT, SCAL, as well as information on well completions and production
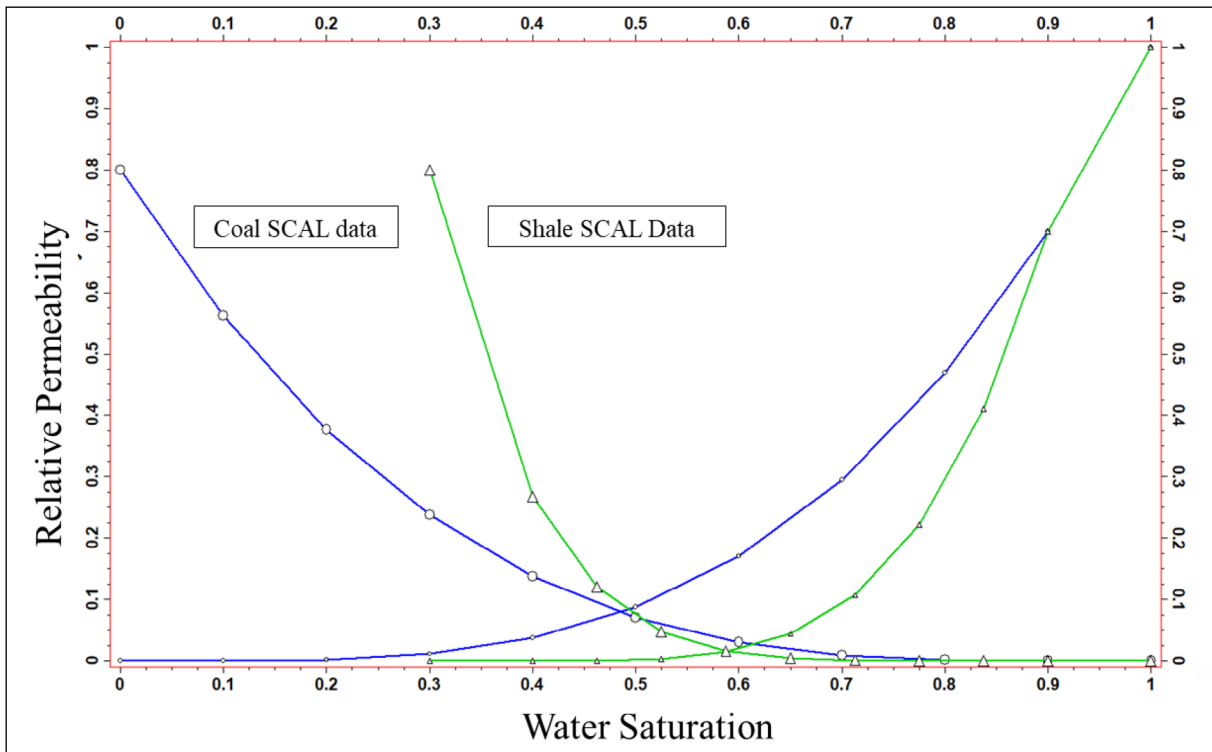
Figure 7- Coal and shale assumed relative permeability data with system gas and water.

Table 1- Relative permeability data used for coal, shale and cleat systems.

	Swc	Sgc	Krw	Krwo	Krg	Krgo	Ng	Nw
Coal	0.1	0.01	1.0	0.7	0.8	0.7	3	3.0
Shale	0.3	0.10	1.0	0.7	0.8	0.7	6	4.0
Cleat	0.0	0.00	1.0	1.0	1.0	1.0	1.0	1.0

constraints. Permeability and porosity values emerge as pivotal factors influencing production performance, as they govern both fluid flow and storage within the reservoir. These properties are intricately linked to the petrophysical characteristics of the coal cleat system.

It is assumed that the coal seams are fully saturated with methane. To estimate the average reservoir pressure, a gradient of 0.433 psi/ft (as outlined in Table 2) has been utilized. This pressure was estimated at the midpoint depth of one of the deepest target seams. In this scenario, the desorption pressure would be equivalent to the reservoir pressure. The deeper coal seams were focused on due to their substantial gas capacity, despite the expectation of lower permeability compared to shallower coals, owing to compaction effects. However, successful hydraulic fracture operations hold the potential to enhance permeability,

Table 2- Table describes all data used to build the base scenario forecast for the study.

Data	Value	Source
Coal density (lb/ft^3)	89	Analysis
Coal Langmuir volume (scf/t)	667	Analysis
ASH content (%)	10	Analysis
Moisture content (%)	3	Analysis
Pressure gradient (psi/ft)	0.433	Assumption
Average reservoir pressure (Psia)	1800	Assumption
Initial water saturation (%)	100	Assumption
Cleat permeability (md)	2	Analysis
Cleat porosity (%)	2	Analysis
Shale data		Petrel default
Coal compressibility (E-6 psia-1)	1.38	Analog
Gas gravity	0.6	Analysis
Water salinity (ppm)	1,200	Analysis

thereby creating a more conducive environment for gas flow towards wellbores.

In each scenario, all wells are positioned to intersect the deepest target coal seams and are equipped with two-stage hydraulic fracturing operations for these primary targets. The parameters of the hydraulic fracture are quantified through simulations utilizing data sourced from Table 3, which is derived from a geomechanical study conducted on a historical well (Figure 8).

The hydraulic fracture can be modelled either using inside built well correlations based on the hydraulic fracture post frack simulation results or using a negative skin which means wells are being stimulated.

The skin factor can be estimated by using the equation 2 below:

$$S = -LN\ [(\alpha * xf)/rw] \qquad (2)$$

The factor α was determined as 0.4 based on a dimensionless fracture conductivity (Fcd) of 13.65,

with a well radius of 0.0889 m and a hydraulic fracture half-length of 145 m. However, the skin factor was estimated to be -3 to model. Figure 9 illustrates the well completion, perforated intervals, and fractured zones.

The Bottom Hole Pressure (BHP) limit was established at a minimum to optimize total production while incorporating the utilization of a downhole water pump. A BHP limit of 10 bars was adopted as a production constraint across all development plan scenarios because of economics of the projects.

The development plan for the wells involves testing various scenarios, taking into account the spatial extent of the study area. It was decided to drill the wells from a single platform because of the difficulties of topography and abundant of forest areas. According to Xiao et al. (2019), the spot drilling pattern (FSWP) scheme has demonstrated promising potential for enhancing CBM recovery from Methane Hydrocarbon Reservoirs (MHR). In this study, a 5-spot well pattern is applied, with all five wells situated on

Table 3- Hydraulic fracture analysis of one of the old well from study area.

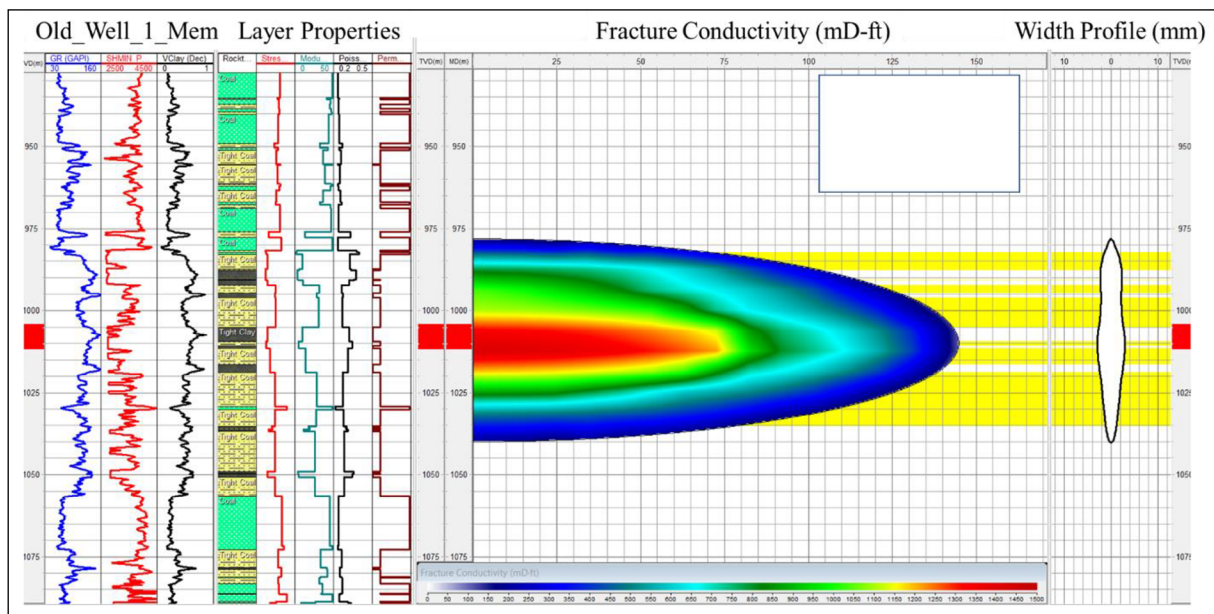| Proppant (T)	HF half length (m)	HF height (m)	HF width (mm)	Avg Conductivity(md.ft)	FCD
80	145	62	3.39	751.2	13.65

Figure 8- Hydraulic fracture post job simulation of a well from Zonguldak.
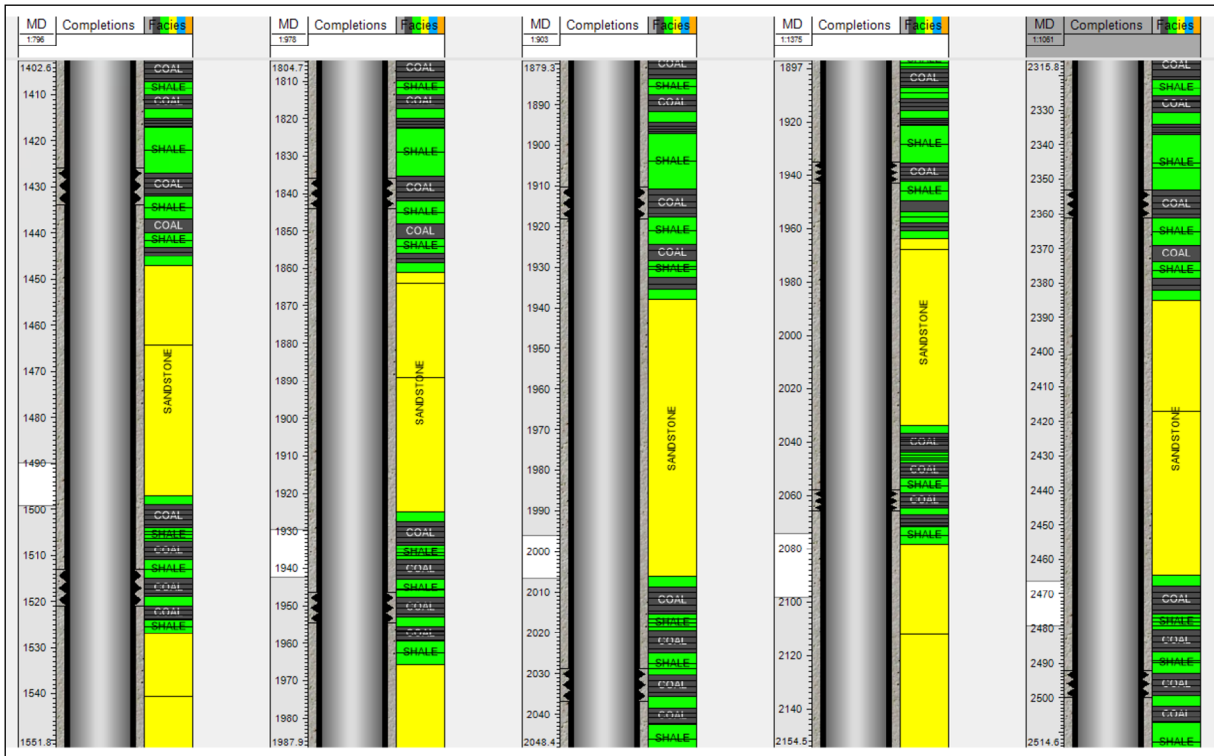
Figure 9- Perforation intervals for hydraulic fracture simulation for 5 wells with two separate coal and shale zones.

the same drilling platform, each targeting a different section of the modelling area. Initially, the distance between wells will be as short as 10 m, gradually increasing up to 600 m at the outer reaches of the well pattern (Figure 10).

3. Discussion

For modelling purposes, vertical and lateral wells were simulated for the pilot project area. Field cumulative gas production and cumulative water production were computed using Eclipse software,
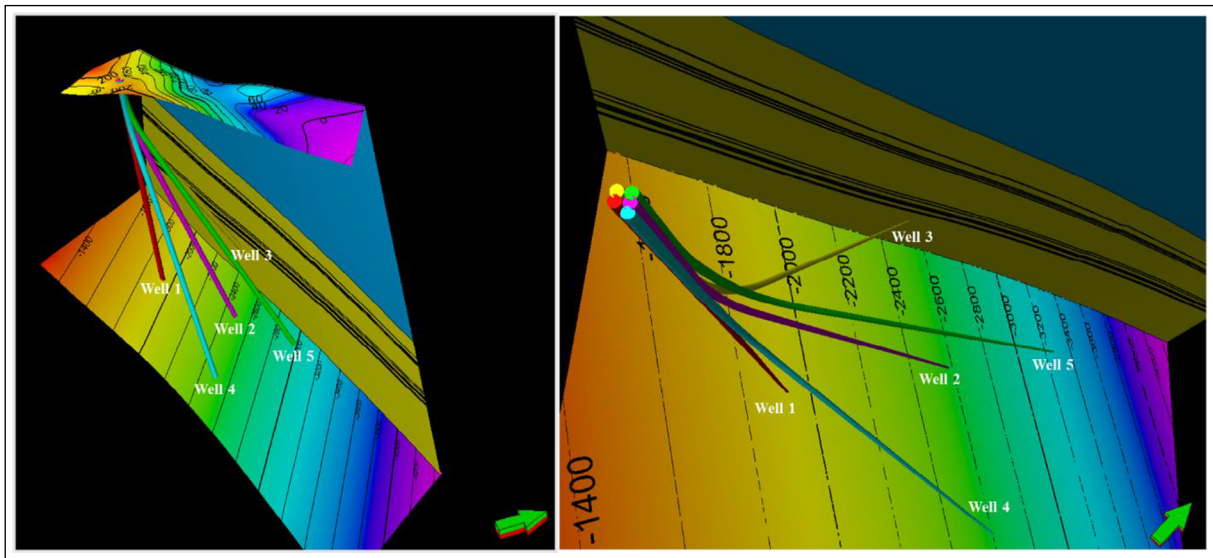

Figure 10- Five spot well pattern on prepared geological model showing coal, shale and other layers.

and the data were plotted and analysed using Petrel Reservoir Engineering. The results of each simulation run are represented as follows.

3.1. Production Profiles of Different Number of Wells

The cumulative gas and water production results for the five scenarios demonstrate that the 5-well configuration yields the highest gas production, totalling 1.803 billion m³. In comparison, the forecasted cumulative gas production for the 4-well, 3-well, 2-well, and single-well scenarios are 1.544 billion m³, 1.339 billion m³, 1.119 billion m³, and 0.704 billion m³ respectively (Figure 11). Analysis of total production values reveals that production does not increase exponentially with the number of wells. However, examination of daily gas production values (Figure 11b) indicates that increasing the number of wells accelerates the transition to peak production due to pressure interference. Moreover, additional wells facilitate more efficient dewatering (Figure 11c, d) of the entire drainage area within a shorter timeframe, thereby enabling the attainment of peak gas production rates more rapidly.

From the scenario of one well to five wells, the total cumulative gas production experiences an almost ninefold increase over a 10-year production period, rising from 0.097 billion m³ to 0.852 billion m³ (Figure 11a). Notably, dewatering with just one well would require more time, potentially limiting the quantity of desorbed gas compared to the five-well spot scenario. Upon examining Figure 11b after 30 years of production, it becomes evident that the daily gas production from a single well surpasses that of the five wells with the production of around 70,000 m³. This phenomenon arises because the one-well scenario has likely depleted most of the water in the formation, thereby entering an efficient gas production phase. Conversely, the five-well scenario has already passed its peak production phase and entered a decline. When considering total production values, the 0.704 billion m³ of production from one well represents approximately 1/2.5 of the 1.803 billion m³ of production from five wells. In this context, while it may not seem logical to drill more than one well, initiating five wells early on appears economically reasonable for realizing early profits in the project.
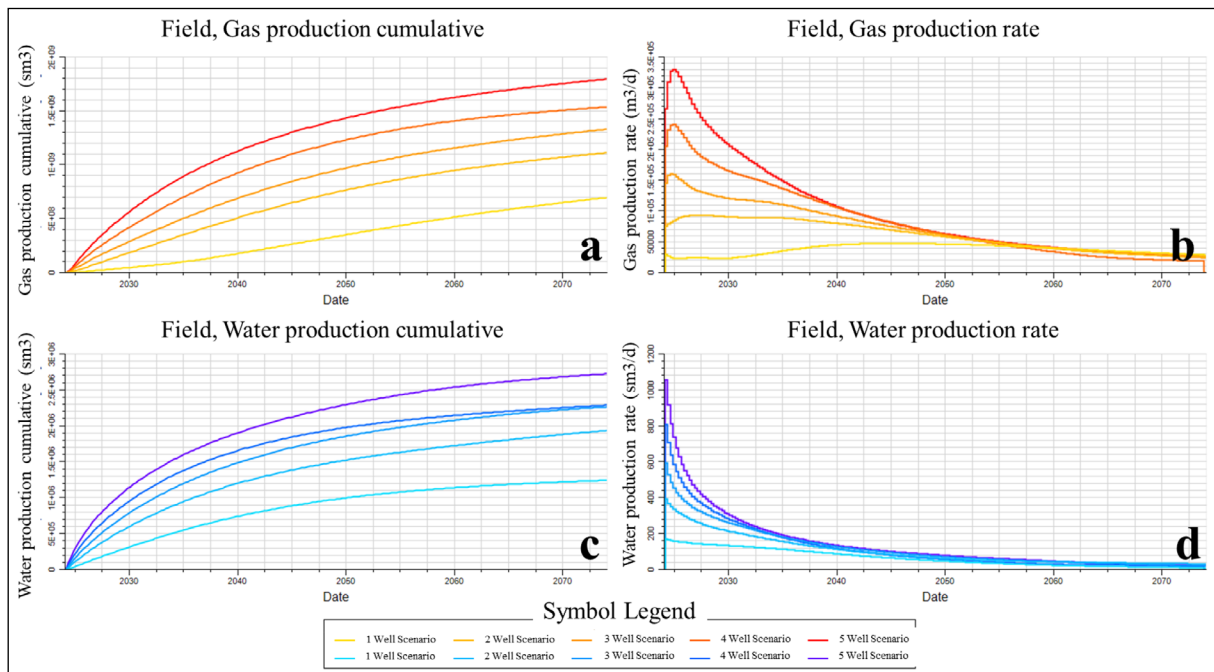

Figure 11- Different number of wells gas and water production forecast for 50 years, a) Gas Production Cumulative (m³), b) Gas Production Daily Rate (m³/d), c) Water Production Cumulative (m³), d) Water production daily rate (m³).

3.2. Individual Gas and Water Production Values of Specific Wells for Different Number of Wells Scenarios

Well 1 serves as the primary gas producer, while Well 2 exhibits lower gas production. Conversely, in terms of water production, Well 2 surpasses Well 1 (Figure 12). This discrepancy can be attributed to the fact that Well 1 is positioned higher up in the target formations, leading to lower water production compared to Well 2, which operates at a lower elevation. When operated together, Well 2 aids in expediting water evacuation from the formations, thus enhancing the gas production from Well 1.

In the scenario involving three wells, Well 3 initially emerges as the most productive, but its productivity diminishes over time, eventually becoming the least productive well (Figure 13f). Concerning water production, Well 3 exhibits similar performance to Well 2, while Well 1 continues to produce less water due to its higher positioning (Figure 14-e, f).
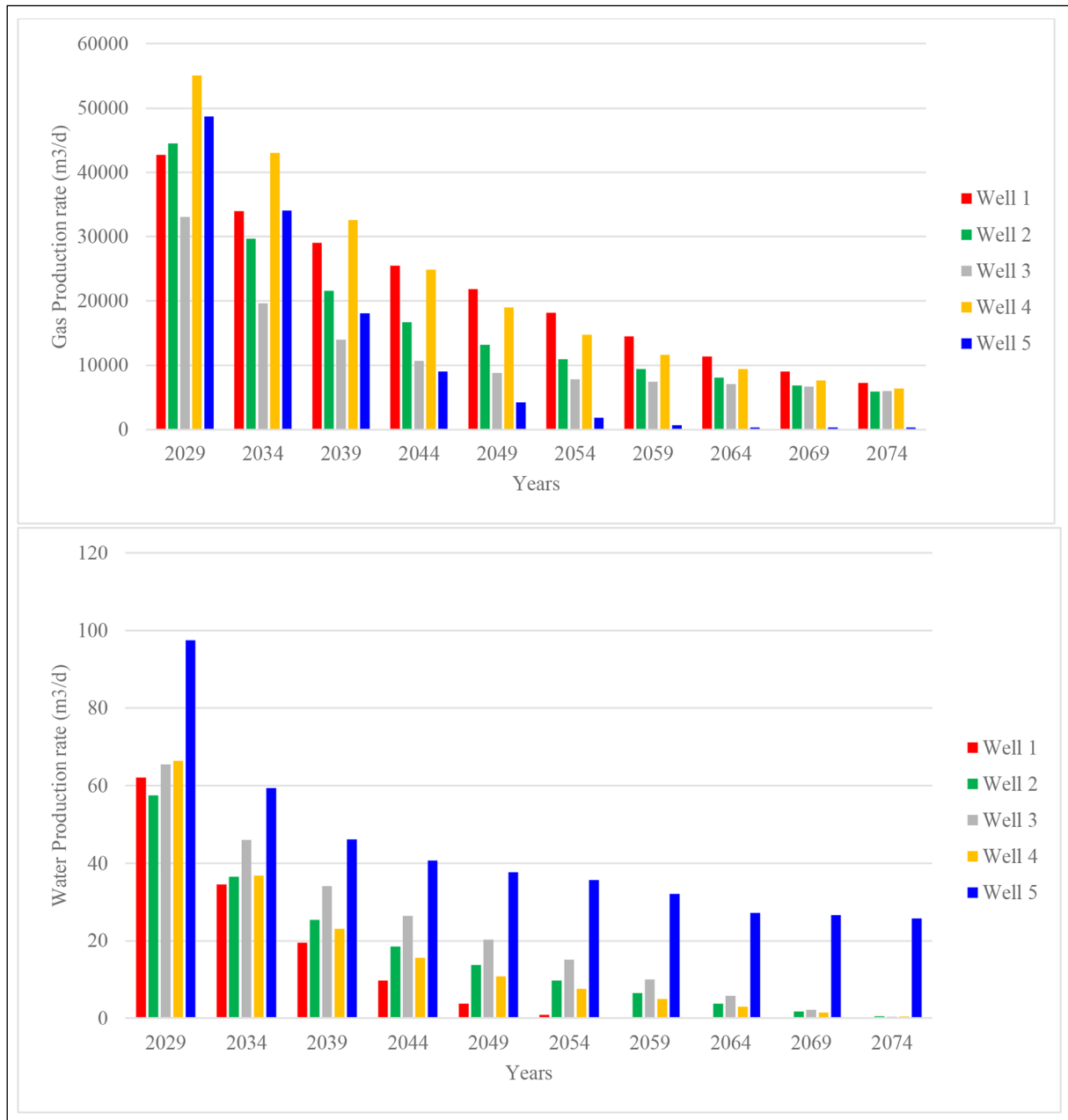

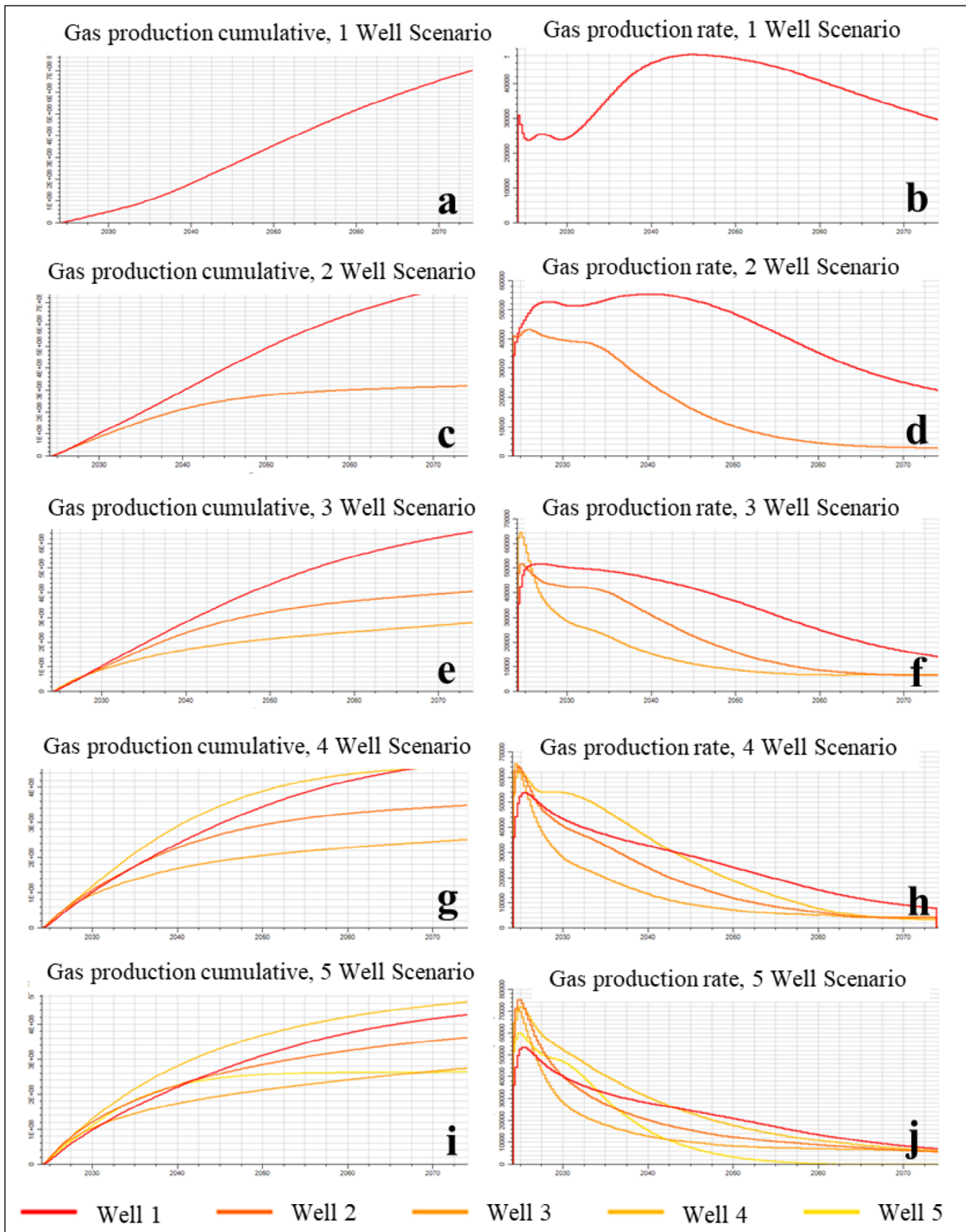Figure 12- Daily gas and water production rate for 5 wells for each 5 years.

Figure 13- Cumulative and daily gas productions of different number of wells scenarios, a) Well 1 Gas Production Cumulative (m³), b) Well 1 Gas Production Daily Rate (m³/d), c) 2 well (Well 1 and 2) Gas Production Cumulative (m³), d) 2 well (Well 1 and 2) Gas Production Daily Rate (m³/d), e) 3 well (Well 1,2 and 3) Gas Production Cumulative (m³) f: 3 well (Well 1,2 and 3) Gas Production Daily Rate (m³/d), g) 4 well (Well 1,2,3 and 4) Gas Production Cumulative (m³), h) 4 well (Well 1,2,3 and 4 Gas Production Daily Rate (m³/d), i) 5 well (Well 1,2,3,4 and 5) Gas Production Cumulative (m³), j) 5 well (Well 1,2,3,4 and 5) Gas Production Daily Rate (m³/d).
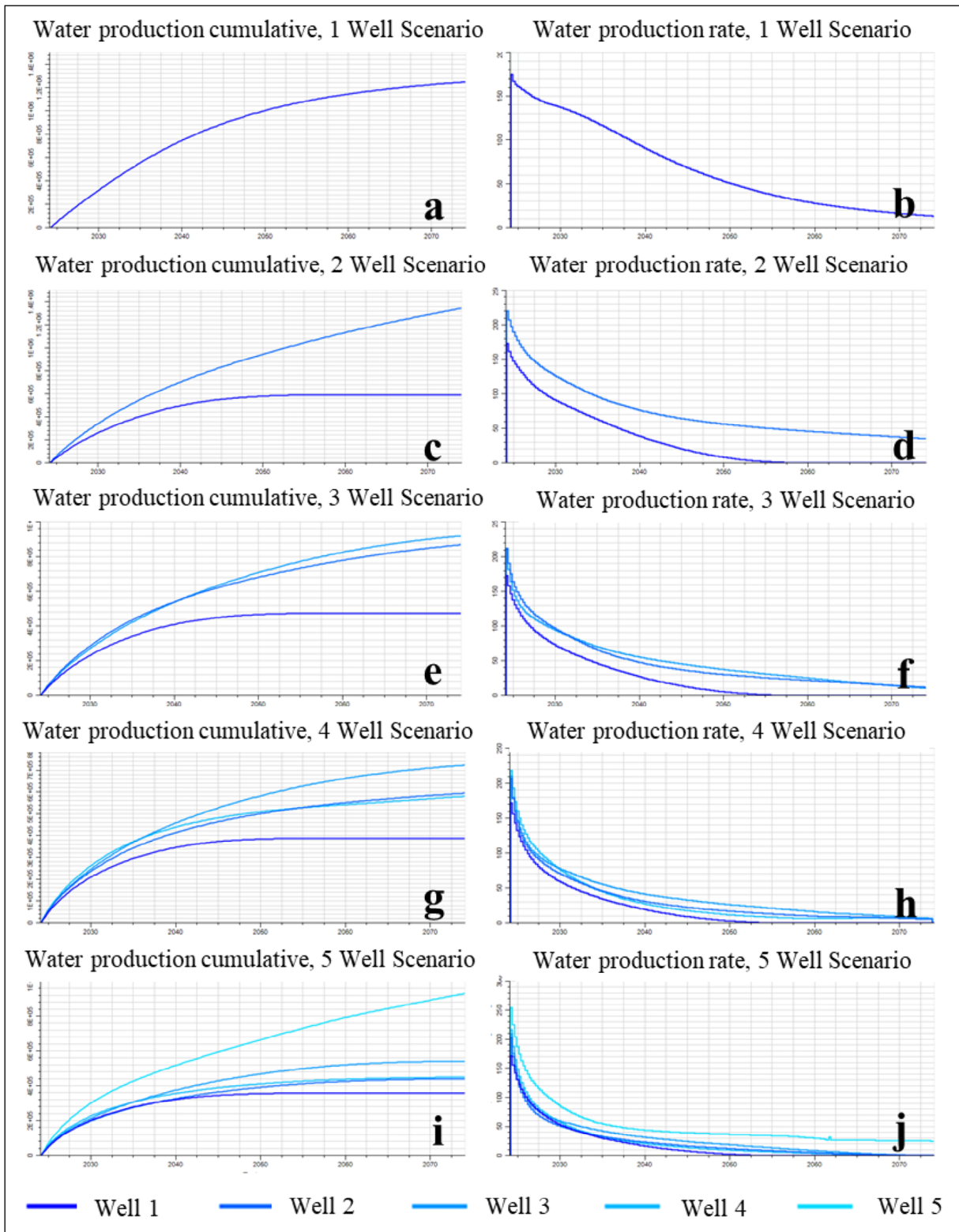
Figure 14- Cumulative and daily water productions of different number of wells scenarios, a) Well 1 Water Production Cumulative (m³), b) Well 1 Water Production Daily Rate (m³/d), c) 2 well (Well 1 and 2) Water Production Cumulative (m³), d) 2 well (Well 1 and 2) Water Production Daily Rate (m³/d), e) 3 well (Well 1,2 and 3) Water Production Cumulative (m³), f) 3 well (Well 1,2 and 3) Water Production Daily Rate (m³/d), g) 4 well (Well 1,2,3 and 4) Water Production Cumulative (m³), h) 4 well (Well 1,2,3 and 4 Water Production Daily Rate (m³/d), i) 5 well (Well 1,2,3,4 and 5) Water Production Cumulative (m³), j) 5 well (Well 1,2,3,4 and 5) Water Production Daily Rate (m³/d).

With the addition of Well 4, peak production increases by 60,000 m³, while the cumulative contribution of the fourth well to water production results in an overall increase of 20,000 m³ across other wells (Figure 13g, h, Figure 14g, h). Similarly, Well 5 contributes 60,000 m³ to gas production, boosting the production of other wells by 30,000 m³ at peak production. Due to its deeper positioning, Well 5 naturally yields more water than the others (Figure 13i, j, Figure 14i, j).

3.3. Gas Production Profiles of the Same Wells in Different Scenarios

Well-1 experiences a significant increase in daily gas production when Well-2 is added to the production scheme (Figure 15b). Subsequent additions of wells result in earlier peak production periods. However, examining the total production over 50 years reveals that Well-1 achieves its optimal potential when
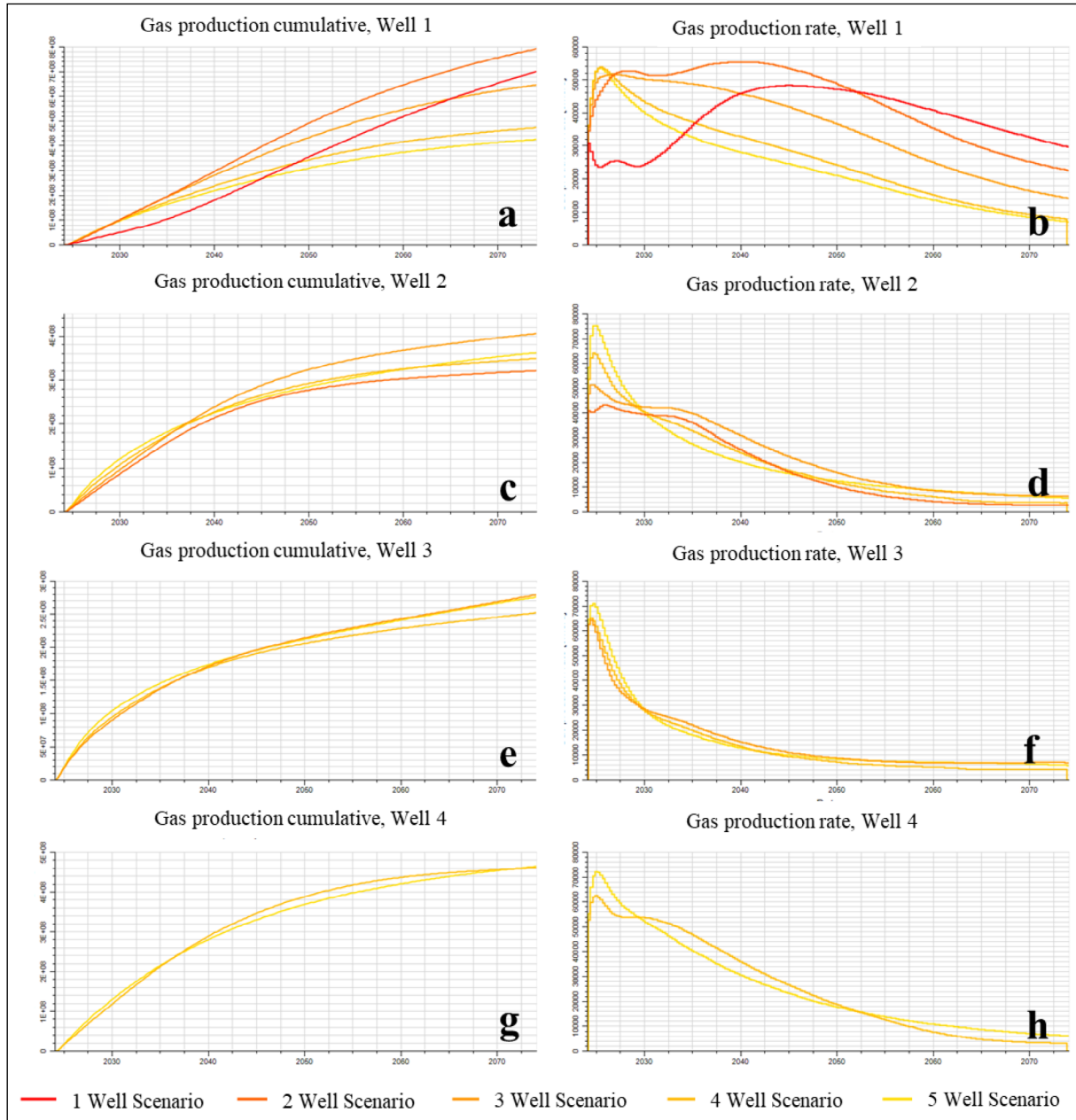

Figure 15- Cumulative and daily gas production of Well 1,2,3 and 4 in different scenarios, a) Well 1 Gas Production Cumulative (m³), b) Well 1 Gas Production Daily Rate (m³/d), c) Well 2 Gas Production Cumulative (m³), d) Well 2 Gas Production Daily Rate (m³/d), e) Well 3 Gas Production Cumulative (m³), f) Well 3 Gas Production Daily Rate (m³/d), g) Well 4 Gas Production Cumulative (m³), h) Well 4 Gas Production Daily Rate (m³/d).

operating in conjunction with Well-2 (Figure 15a). Daily gas production values for Well-2 exhibit steady increases with the addition of each new well (Figure 15d). However, its best performance over the 50-year period occurs when it is in production alongside Well-1 (Figure 15c). Well-3 and Well-4 demonstrate marginal production increases with the introduction of new wells (Figure 15e, f, g, h).

3.4. Pressure and Gas Saturation Change Over Time

Pressure and gas saturation maps were generated using Petrel to monitor changes in target coal levels every 10 years. Figure 16 illustrates the gradual

decline in field pressure over time due to ongoing gas and water extraction activities.

Figure 17 depicts the anticipated gas saturation across the entire field, indicating that in 2024, saturation levels are expected to reach 100%. Following peak production in the first decade, gas saturation peaks in 2034, particularly near the wells. However, in subsequent years, gas saturation gradually decreases, especially around Well 5 in 20 years, with withdrawal activities shifting to other wells in 30 years. In 40 and 50 years, the remaining gas production is primarily concentrated in the upper
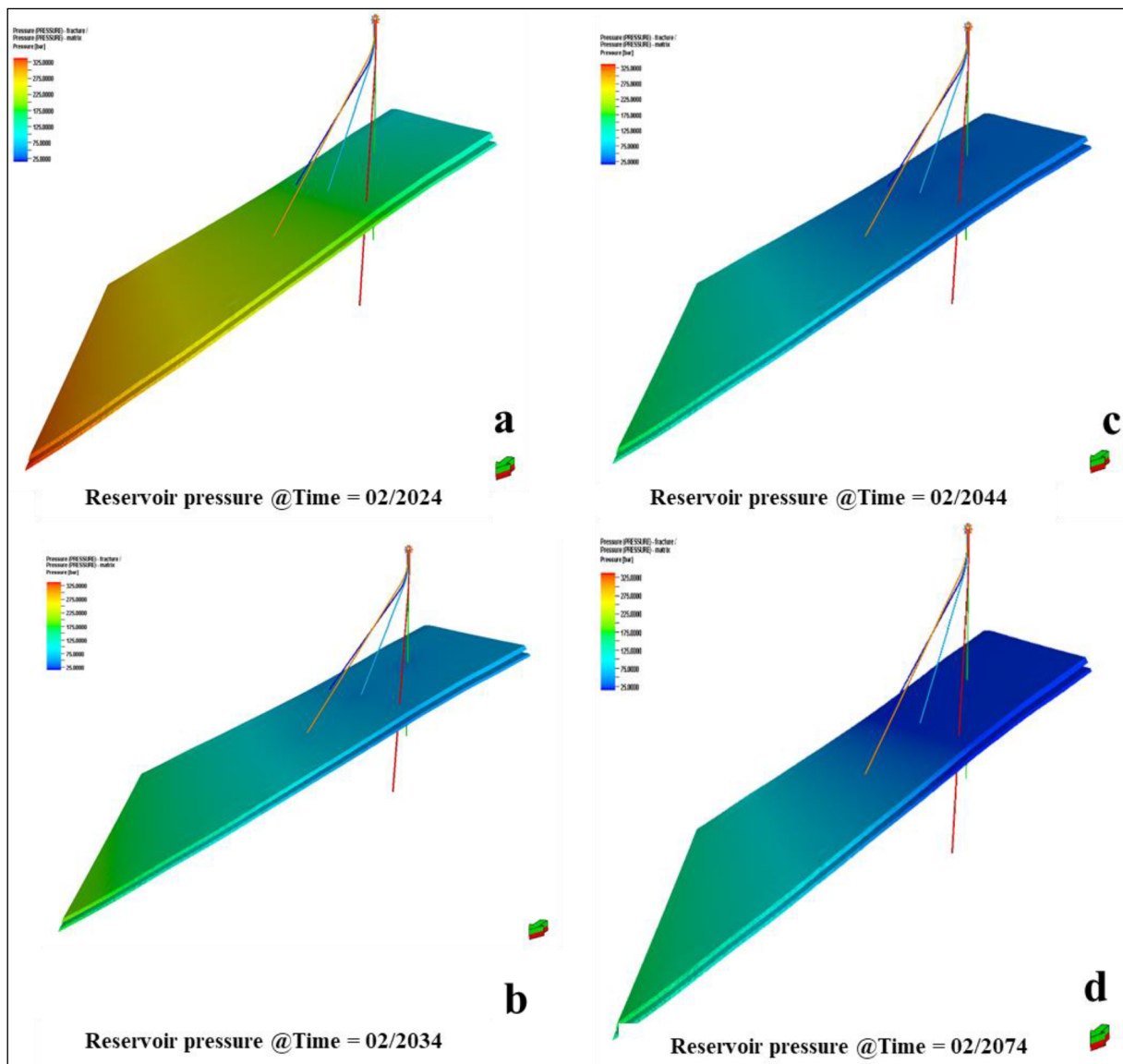

Figure 16- Pressure change over time, a) Reservoir pressure at 02/2024, b) Reservoir pressure at 02/2034, c) Reservoir pressure at 02/2044, d) Reservoir pressure at 02/2074.
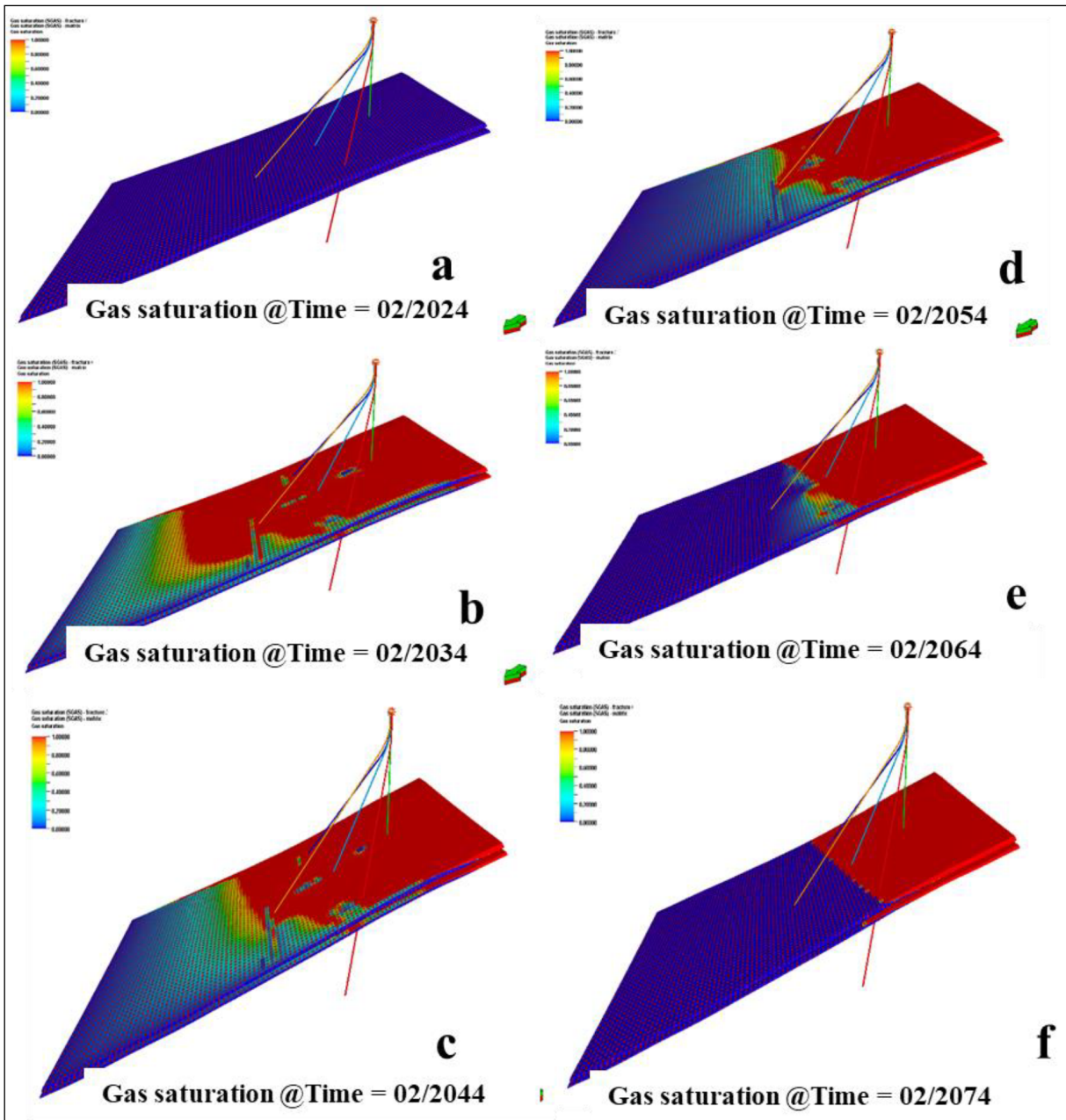
Figure 17- Gas Saturation change over time, a) as Saturation at 02/2024, b) Gas Saturation at 02/2034, c) Gas Saturation at 02/2034, d) Gas Saturation at 02/2044, e) Gas Saturation at 02/2054, f) Gas Saturation at 02/2074.

wells, with minimal production from the deeper wells. Despite the apparent high gas saturation, actual gas production rates remain relatively low as the project progressed.

4. Results

This study was undertaken to assess coalbed methane potential of the Karadon region, known as one of the most promising areas for gas exploration within Türkiye's Zonguldak coal basin, renowned for

its long-established gas reserves. The study followed a structured workflow, beginning with geological modelling and reservoir characterization using digital data sourced from nearby coal galleries. Nine distinct coal seam levels and shale layers were systematically divided into individual layers, creating a detailed 3D model using the Petrel (2022.1) software. To achieve a high-resolution model, coal layers were subdivided into 1 m or finer segments, while shale levels were segmented into layers of at least 2 m, sometimes

thinner. This approach resulted in a comprehensive model comprising 121 layers, covering the entire area and divided into 635,613 grid cells.

Schlumberger's Petrel Reservoir Engineering and Eclipse software were instrumental in creating the dynamic model based on the prepared data. This included inputting gas composition, PVT characteristics, and SCAL data into the software.

To optimize drainage across the entire area while maintaining practicality, field studies were conducted to determine optimal well locations. Given the challenging terrain characterized by dense mountains and forests, a single location was chosen for efficiency. Based on production forecast studies indicating optimal efficiency with five wells, the widely recognized "5 spot wells" method from literature was adopted. Mechanical earth modelling and hydraulic fracturing simulations were executed using log data retrieved from a previously drilled well in the region. This data facilitated the creation of hydraulic fracturing parameters for two potential levels within all five wells. Subsequent simulations conducted in Eclipse yielded production values for five different scenarios. The results revealed the following cumulative gas and water production for each scenario: the five-well scenario yielded the maximum gas production, totalling 1.803 billion m³. Comparatively, the four-well scenario forecasted 1.544 billion m³, the three-well scenario anticipated 1.339 billion m³, the two-well scenario projected 1.119 billion m³, and the single-well scenario estimated 0.704 billion m³. These findings underscore the efficiency and effectiveness of utilizing the 5 spot wells method for maximizing gas production in the Karadon region.

Furthermore, an analysis of individual production values for each well in every scenario was conducted. It was noted that production increased incrementally with each additional well, starting from a single well, and the peak production phase was achieved more rapidly. This acceleration in production can be attributed to the collaborative effort of the wells in reducing hydrostatic pressure more efficiently, thereby optimizing drainage in the region.

The results may deviate from presented results, if more analysis is done on the field. The methodology followed in this study can also be applied to other blocks in the Karadon region. Thus, static, and dynamic reserve calculations can be made realistically in high resolution, from small to large scale. Additionally, calculated production forecast values can be converted into economic analysis.

References

Baltaş, A. 2018. Metan potential and methane production studies of Zonguldak Basin. Proceedings of the 21st International Coal Congress of Turkey, 125-137.

Barış, K., Keleş, C., Ripepi, N., Luxbacher, K., Gürpınar, S., Karmis, M. 2016. The first commercial coal bed methane project in Türkiye - reservoir simulation and prefeasibility study for the Amasra coalfield. International Journal of Oil, Gas and Coal Technology 13, 170.

Clarkson, C.R., Rahmanian, M., Kantzas, A., Morad, K. 2011. Relative permeability of CBM reservoirs: Controls on curve shape. International Journal of Coal Geology 88, 204–217.

Fişne, A., Esen, O. 2014. Coal and gas outburst hazard in Zonguldak Coal Basin of Türkiye, and association with geological parameters. Natural Hazards 74, 1363–1390.

Gürdal, G., Yalçın, M. N. 2000. Gas adsorption capacity of Carboniferous coals in the Zonguldak basin (NW Türkiye) and its controlling factors. Fuel 79, 1913–1924.

Hoşgörmez, H. 2007. Origin and secondary alteration of coalbed and adjacent rock gases in the Zonguldak Basin, western Black Sea Türkiye. Geochemical Journal 41, 201–211.

Langmuir, I. 1918. The adsorptıon of gases on plane surfaces of glass, mica and platinum. Journal of the American Chemical Society 40, 1361–1403.

Laubach, S. E., Marrett, R. A., Olson, J. E., Scott, A. R. 1998. Characteristics and origins of coal cleat: A review. International Journal of Coal Geology 35, 175–207.

Law, D. H. S., van der Meer, L. G. H., Gunter, W. D. 2002. Numerical Simulator Comparison Study for Enhanced Coalbed Methane Recovery Processes, Part I: Pure Carbon Dioxide Injection (WWW Document). onepetro.org.

Puri, R., Evanoff, J. C., Brugler, M. L. 1991. Measurement of Coal Cleat Porosity and Relative Permeability Characteristics. All Days.

Scott, A. R., Kaiser, W. R., Ayers, W. B. J. 1994. Thermogenic and Secondary Biogenic Gases, San Juan Basin, Colorado and New Mexico--Implications for Coalbed Gas Producibility. AAPG Bulletin 78.

Serpen, U., Alpkaya, E. N., Özkan, E. 1998. Preliminary Investigation of Coalbed Methane Potential of the Zonguldak Basin in Türkiye. 9th Turkish Petroleum Congress, Ankara.

Sıyanuç, Ç., Gümrah, F. 2009. Modeling of ECBM recovery from Amasra coalbed in Zonguldak Basin, Türkiye. International Journal of Coal Geology 77, 162–174.

Warren, J. E., Root, P. J. 1963. The Behavior of Naturally Fractured Reservoirs. Society of Petroleum Engineers Journal 3, 245–255.

Xiao, C., Meng, Z., Tian, L. 2019. Semi-analytical modeling of productivity analysis for five-spot well pattern scheme in methane hydrocarbon reservoirs. International Journal of Hydrogen Energy 44, 26955–26969.

Yalçın, M. N., İnan, S. 2002. Carboniferous coals of the Zonguldak basin (northwest Türkiye): Implications for coalbed methane potential. AAPG Bulletin 86.

Yalçın, M. N., İnan, S., Hoşgörmez, H., Çetin, S. 2002. A new Carboniferous coal/shale driven gas play in the Western Black Sea Region (Türkiye). Marine and Petroleum Geology 19, 1241–1256.

Yalçın, M.N., Schenk, H.J., Schaefer, R.G. 1994. Modelling of gas generation in coals of the Zonguldak Basin (northwestern Türkiye). International Journal of Coal Geology 25, 195–212.